Numerically Modelling the Solar Corona

With a Magnetofrictional model

Mayukh Panja, Dibyendu Nandy
CESSI, IISER Kolkata, India
mayukhpanja@gmail.com, dnandi@iiserkol.ac.in

Introduction

The solar corona spews out vast amounts of magnetized plasma into the heliosphere which has a direct impact on the Earth's magnetosphere. Thus it is important that we develop an understanding of the dynamics of the solar corona. Currently it is not possible to observe the 3D magnetic field structure of the solar corona; this warrants the use of numerical simulations to study the coronal magnetic field. Full MHD simulations of the global coronal field, apart from being computationally very expensive would be physically less transparent, owing to the large number of free parameters that are typically used in such codes, which brings us to the Magneto-frictional model which is relatively simpler and computationally more economic.

The Magnetofrictional Model

The Magnetofrictional method uses the fact that magnetic pressure in the corona is greater than the gas pressure. Owing to this low plasma $beta$ the only driving force in the corona is assumed to be the Lorentz force ($\mathbf{J}\times\mathbf{B}$). The induction equation is solved in the vector potential ($\mathbf{A}$),

$$\frac{\partial \mathbf{A}}{\partial t} = \mathbf{v}\times\mathbf{B} - \eta_c \mathbf{j}, \tag{1}$$

$$\mathbf{v} = \frac{1}{\nu}\frac{\mathbf{J}\times\mathbf{B}}{B^2} + v_0 e^{(2.5R_\odot - r)/r_w}\hat{\mathbf{r}} \tag{2}$$

The second term in equation (3) models the solar wind, which opens up the magnetic field lines as they reach the Source Surface

Numerical method

Our computational domain is a $101\times161\times360$ grid. Grid specifications are as follows, $1R_\odot < r < 2.5R_\odot$, $10^o \le \theta \le 170^o$, $0 \le \phi \le 360^o$, $\triangle r = 0.015R_\odot$, $\triangle\theta = \triangle\phi = 1^o$. We solve the equations in spherical polar co-ordinates. The variables have been defined on a staggered grid, to prevent spatial odd-even decoupling of grids in the second derivative. $\mathbf{A}$ and $\mathbf{J}$ have been defined on the cell ribs, $\mathbf{B}$ on the cell faces and $\mathbf{v}$ on the cell vertices. For example,

$$A^\theta \longrightarrow A^{r,\theta+\frac{1}{2},\phi}$$
$$B^\theta \longrightarrow B^{r+\frac{1}{2},\theta,\phi+\frac{1}{2}}$$
$$v^\theta \longrightarrow v^{r,\theta,\phi}$$

To find $\mathbf{J}$ and $\mathbf{B}$ on the cell vertices before calculating $\mathbf{v}$, linear interpolations have been used. A Van Leer Slope Limiter has been used to interpolate $\mathbf{B}$ onto the cell ribs, before calculating $\mathbf{v}\times\mathbf{B}$. A second order accurate central difference scheme has been used to calculate $\nabla\times\mathbf{A}$ and $\nabla\times\mathbf{B}$. Integration in time has been done by a first order accurate Euler method.

Simulation results

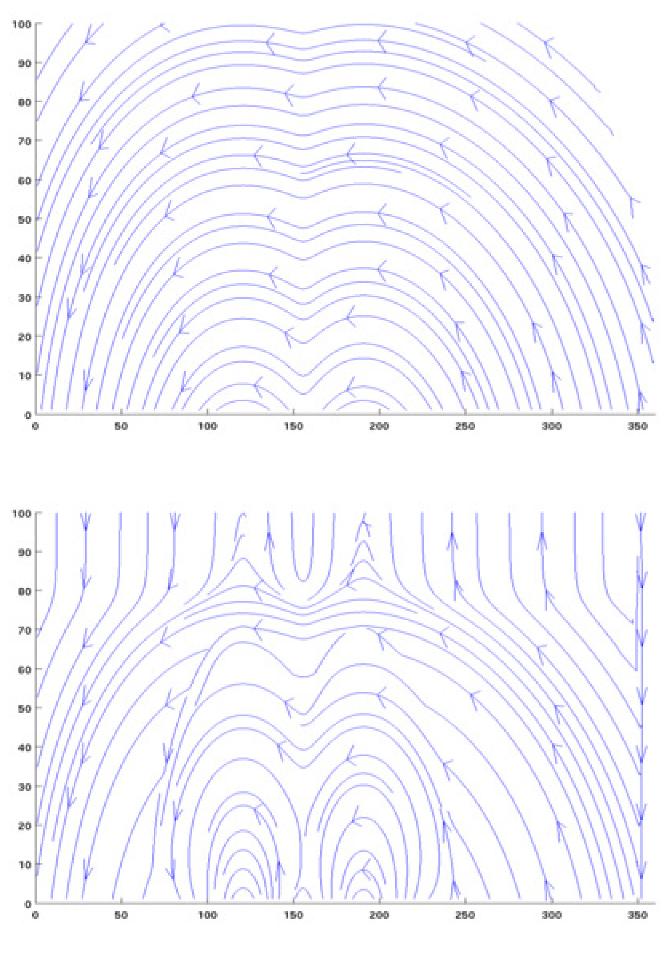

Figure 1: Evolution of field lines projected on the r-phi plane at theta = 180^0

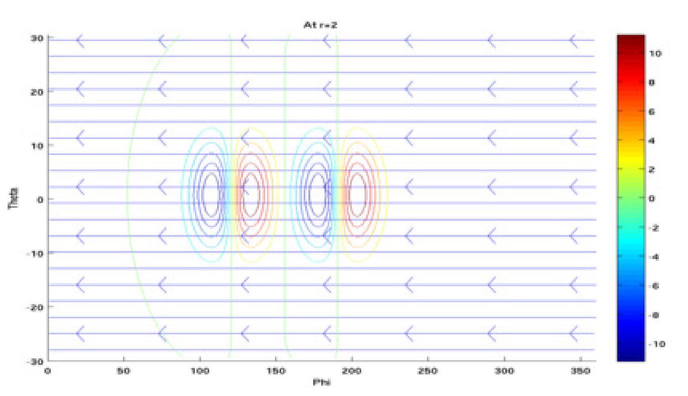

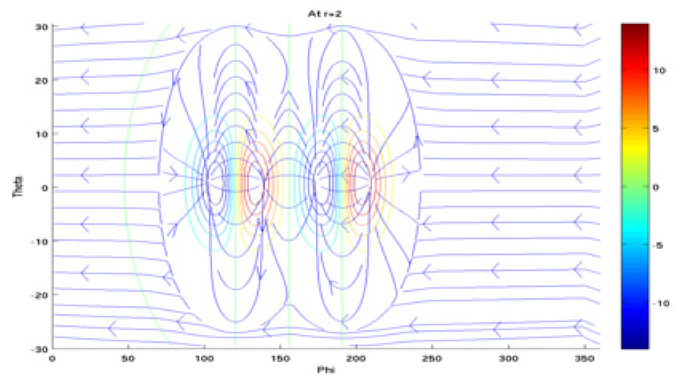

Figure 2: Evolution of field lines projected on the theta-phi plane at r=1.015 $R_\odot$

Discussion

The main purpose of this trial run was to test the validity of the code.
The bipoles, which initially have a lot of concentrated current, expand and relax towards a force-free equilibrium. This is evident from figures 1 and 2. As field lines of the adjacent bipoles expand, opposing field lines come close to each other and small zones of high current are formed. The field lines reconnect to get rid of the excess current and cross connections between the adjacent bipoles are formed over the external Polarity Inversion Line. This is more evident from Figure 2 which plots the field lines at r=1.015 $R_\odot$.

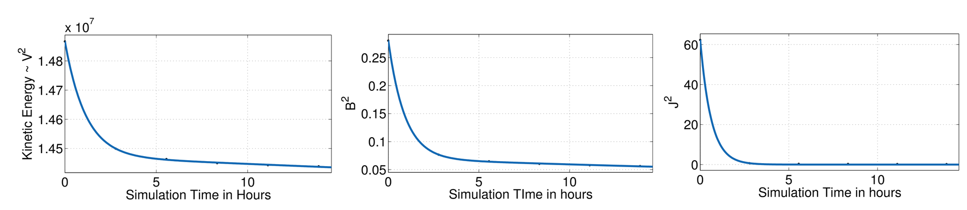

Figure 3: Integral of kinetic energy, magnetic energy and J^2 over the entire computational volume versus time.

Quadrupolar Arrangement of spots

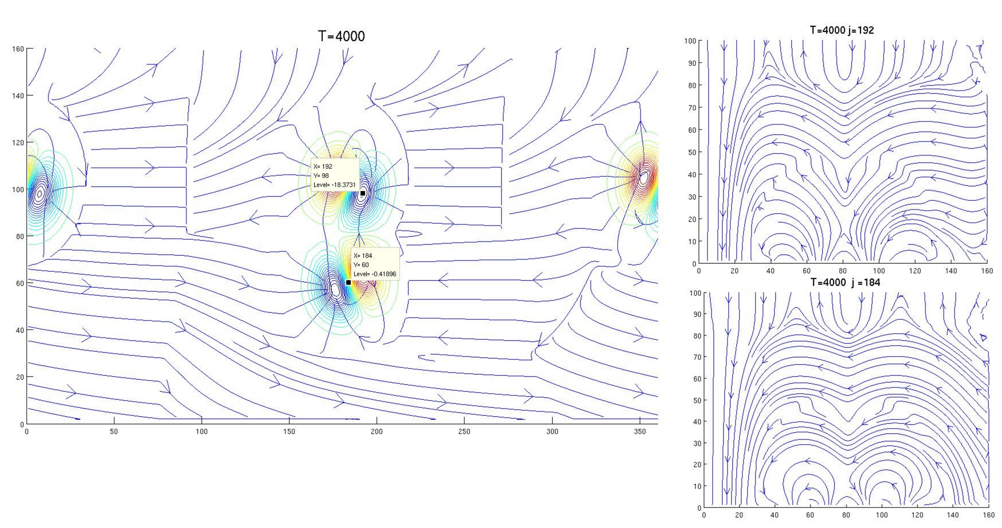

Figure 4: The theta-phi plane at r=1.015 $R_\odot$ and the r-theta planes at two different longitudes at T=4000 (code unit).

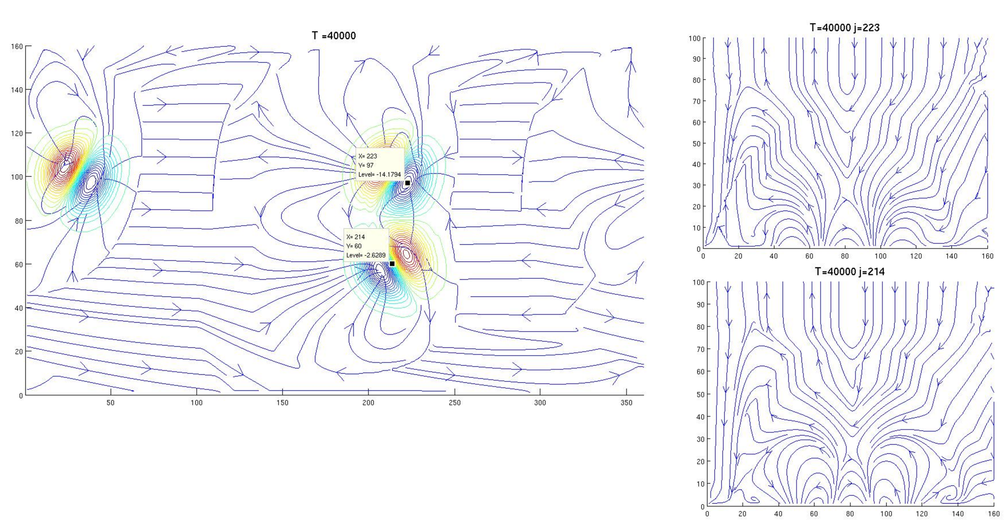

Figure 5: The theta-phi plane at r=1.015 $R_\odot$ and the r-theta planes at two different longitudes at T = 40000 (code unit).

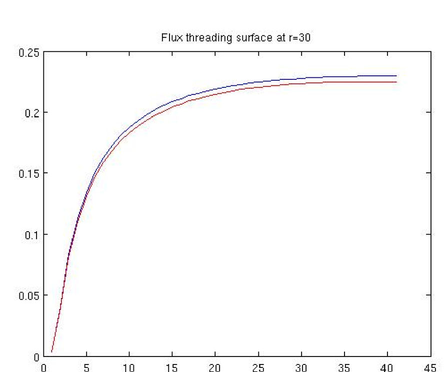

Figure 6: Plot of the flux threading the theta-phi plane at r = 1.45 $R_\odot$.

A uniform velocity has been applied in the phi direction. This has been done to test the periodic boundary condition. In the absence of any shearing photospheric motion, the field lines relax to a force free state - cross connections and open field lines are formed, thereby increasing the open flux at r=1.45 $R_\odot$.

Surface Flux Transport Model

We further develop a Surface Transport Flux model in the Vector potential which can be used to drive the coronal model for simulating long time periods.

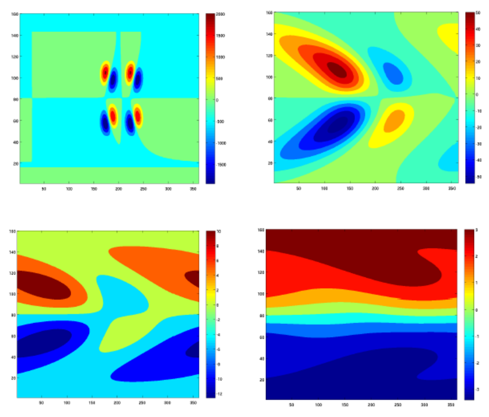

Figure 7: Evolution of the photospheric magnetic field in response to differential rotation and meridional flow.

Twisting Photospheric Motion

We apply a twisting photospheric velocity on one of the bipolar regions.

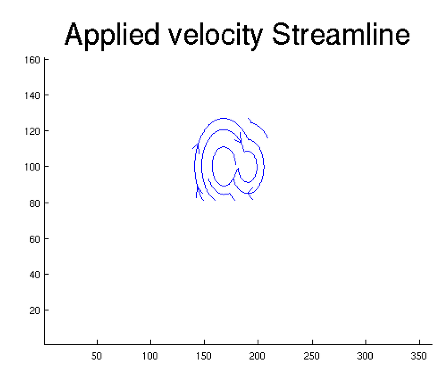

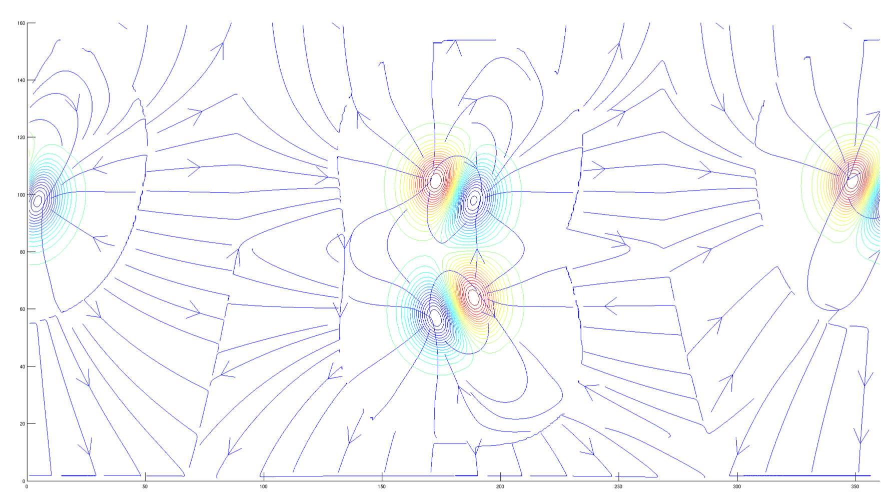

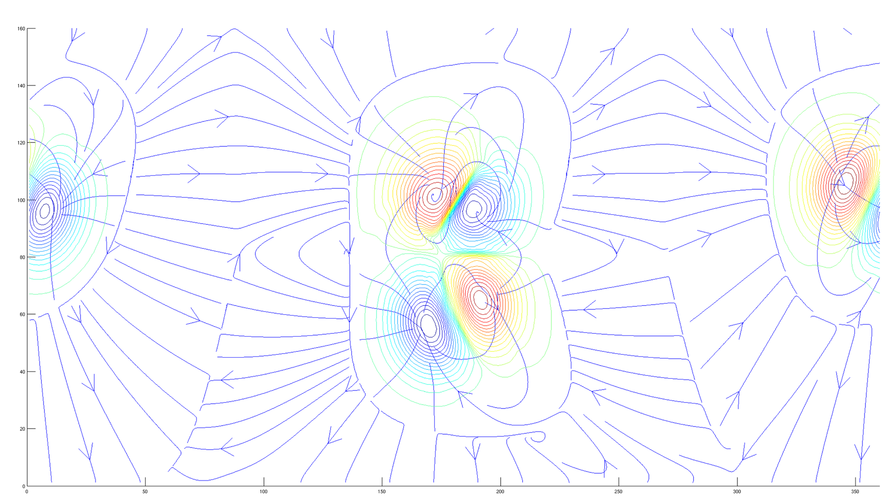

The field lines are twisted in response to the applied photospheric motion and we see sigmoidal structures forming above the internal Polarity Inversion Line.

Future Work

We plan to use this model for full solar cycle, data driven simulations of the corona.

References

[1] Yang, W. H., Sturrock, P. A., Antiochos, S. K. 1986, ApJ , 309: 383-391
[2]van Ballegooijen,Priest, E. P, Macay, D. H., 2000, ApJ, 539:983-994
[3] A.R. Yeates, D.H. Mackay, A.A. van Ballegooijen Solar Phys(2007) 245:87-107
[4] Macay, D. H., van Ballegooijen, 2006, ApJ, 641:577-589
[5] Mark C.M. Cheung, Marc L. DeRosa., 2012, ApJ,757:147

Acknowledgemet

We acknowledge funding for our research from the Ministry of Human Resource Development and CEFIPRA through CESSI. We are also grateful to Mark Cheung,LMSAL for useful discussions during the development of this code.